PHYSICAL REVIEW B **94**, 205406 (2016)

Momentum-resolved hot electron dynamics at the 2*H*-MoS_2 surface

P. Hein,[1] A. Stange,[1,*] K. Hanff,[1] L. X. Yang,[1,2] G. Rohde,[1] K. Rossnagel,[1] and M. Bauer[1]

[1]*Institut für Experimentelle und Angewandte Physik, Christian-Albrechts-Universität zu Kiel, D-24098 Kiel, Germany*

[2]*Physics Department, Tsinghua University, Beijing 100089, People's Republic of China*

(Received 24 June 2016; published 7 November 2016)

Time- and angle-resolved photoelectron spectroscopy (trARPES) is employed to study hot electron dynamics in the conduction band of photoexcited 2*H*-MoS_2. Momentum-dependent rise times of up to 150 fs after near-ultraviolet photoexcitation and decay times of the order of several-hundred fs allow us to locate areas of light absorption in the conduction-band energy landscape as well as to track the relaxation of hot electrons into the lowest-energy states. The conduction-band minima are finally depopulated within ≈1 ps, although a residual population remains up to the maximum investigated pump-probe delay of 15 ps. The presence of the fast depopulation channel differs from the results of experiments of bulk MoS_2 performed with all-optical methods. It conforms, however, with recent findings for monolayer MoS_2. We attribute this similarity to defect and surface states being of considerable relevance for the near-surface electron dynamics of bulk MoS_2, as probed in a trARPES experiment.

DOI: 10.1103/PhysRevB.94.205406

I. INTRODUCTION

Molybdenum disulfide (MoS_2) belongs to the family of layered transition-metal dichalcogenides (TMDCs). The basic building blocks of TMDCs are sandwiches composed of a hexagonal transition-metal layer (here, Mo) covalently bonded on both sides to hexagonal chalcogen layers (here, S). A three-dimensional crystal is finally formed by stacking the sandwiches on top of each other, as illustrated for the centrosymmetric phase of MoS_2 (2*H*-MoS_2) in Fig. 1(a). Bulk 2*H*-MoS_2 is an indirect gap semiconductor exhibiting a gap energy of $E_{gap} = 1.29$ eV [1]. Recently, few-layer and monolayer samples of MoS_2 (and other TMDCs such as WSe_2 and WS_2) have attracted considerable interest because of their exceptional electronic and optical properties that distinctly differ from what is observed for bulk samples [2–6]. These peculiarities arise in large part from a transition from an indirect to a direct band-gap semiconductor ($E_{gap} \approx 1.8$ eV) when thinning MoS_2 to a single sandwich [7,8]. This makes monolayer MoS_2 a promising candidate for future applications in electronics, photovoltaics, and photonics [2]. Additionally, as a result of the noncentrosymmetric character of MoS_2 monolayers, a (spin-)selective population of degenerate conduction-band minima by circularly polarized light becomes possible, which is potentially useful for the realization of valleytronic and spintronic devices [9,10]. Notably, this type of spin selectivity is conserved within the individual sandwiches of bulk 2*H*-MoS_2 and other TMDCs even though the overall crystalline structure is centrosymmetric [11]. Photoemission spectroscopy is capable of probing such effects owing to its high surface sensitivity, virtually probing the topmost sandwich of a bulk sample as demonstrated in recent photoemission and time-resolved photoemission studies of 2*H*-MoS_2 [12] and 2*H*-WSe_2 [13,14].

As electronic and optoelectronic properties of semiconductors, such as charge transport, quantum efficiency, and polarization decay, are in general governed by the fundamental processes of carrier relaxation [16], many time-domain studies of few-layer and monolayer MoS_2 as well as the bulk parent compound 2*H*-MoS_2 have been conducted recently [17–31]. Various characteristic time scales are reported in these studies, allowing for a classification of different processes taking place on a sub-100 fs, a 100 fs, a few picosecond, and a 10–100 ps time scale, respectively. Furthermore, in the case of bulk MoS_2, even nanosecond dynamics has been observed [29,30]. These studies have been performed almost exclusively using time-resolved all-optical spectroscopy (trAOS) techniques and have provided a comprehensive view of the complex carrier and lattice dynamics of MoS_2 involving carrier intra- and intervalley scattering, defect capture, and carrier recombination. The disentanglement of the different relaxation processes from this type of measurement is, however, not necessarily straightforward because the optical probe signal intrinsically mixes electron and hole dynamics. Furthermore, the inherent lack of momentum resolution of these techniques can result in a signal integrating over different decay channels, which makes multiexponential fits necessary and the data interpretation potentially ambiguous. Alternative, less comprehensive time-domain techniques, which address the different aspects of carrier relaxation more selectively, can complement these studies and may provide additional information toward a profound understanding of carrier dynamics in these materials.

Time- and angle-resolved photoelectron spectroscopy (trARPES) is the most direct technique to resolve hot electron dynamics in solids after absorption of an ultrafast laser pulse. It particularly allows one to map electronic processes on their fundamental time scales with high momentum and energy resolution [32–34]. Furthermore, as a photoemission spectroscopy technique, trARPES is highly surface sensitive, i.e., in general only photoelectrons emitted from the topmost layers of a bulk sample contribute to the photoemission signal. So far, two time-resolved photoemission studies of MoS_2 compounds related to the present work have been reported. In a time-resolved two-photon photoemission experiment, Tanaka *et al.* studied hot electron relaxation in 2*H*-MoS_2 [35]. The photon energy of the probe pulse used in this study, however, limited the accessible momentum range considerably so that

*stange@physik.uni-kiel.de

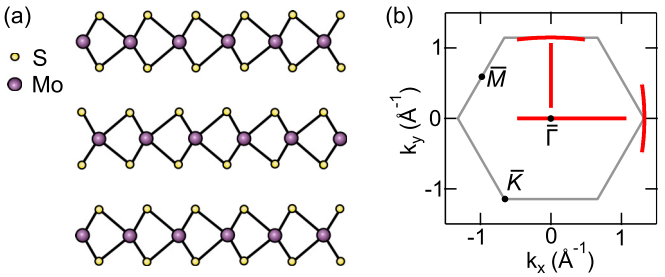

FIG. 1. (a) Side view of the $2H_b$ crystal structure of bulk MoS_2 [15]. $2H$-MoS_2 consists of covalently bonded S-Mo-S layers that are held together via van der Waals–like interactions. (b) Surface-projected Brillouin zone of $2H$-MoS_2. The momentum cuts investigated in the present study are indicated by red lines.

only the carrier dynamics in the vicinity of the Γ point could be probed. Cabo *et al.* used trARPES in order to study the carrier relaxation of single-layer MoS_2 grown on Au(111) [24]. The reported results are, however, dominated by the interaction with the gold substrate so that conclusions on relaxation mechanisms intrinsic to MoS_2 could not be drawn. Due to the lack of sufficiently large sheets of exfoliated MoS_2, trARPES measurements on substrate-decoupled (suspended) MoS_2 monolayers have not been reported yet. Closely related to our work is finally a time-resolved momentum-integrated photoemission study of bulk $MoSe_2$ and bulk WSe_2 by Rettenberger *et al.* [36]. In both materials, a biexponential decay of the conduction-band population was observed with characteristic time scales of 1–2 ps and 3–5 ps, respectively. These results were interpreted in terms of an energy-dependent diffusion of the photoexcited electrons from the surface into the bulk.

In this work, we present energy- and momentum-resolved data of hot electron dynamics in $2H$-MoS_2 measured by trARPES along different directions within the first Brillouin zone. Photoemission spectra were taken along the high-symmetry directions $\bar{\Gamma}\bar{K}$ and $\bar{\Gamma}\bar{M}$, as well as along lines centered on $\bar{K}$ and $\bar{M}$, perpendicular to $\bar{\Gamma}\bar{K}$ and $\bar{\Gamma}\bar{M}$ lines, respectively [see Fig. 1(b)]. Our analysis of the photoemission data yields momentum-resolved carrier population, relaxation, and depopulation times for the conduction band following excitation with 31 fs, 395 nm laser pulses. By correlating the observed carrier dynamics with the results of band structure calculations, we are able to locate the hot spots of the nascent electron population generated by interband absorption, track carrier relaxation pathways into valleys of the conduction band, and, finally, follow the depopulation of the conduction-band minima. Notably, our data show that at least two different decay channels contribute to the depopulation of the conduction band. The major part of the population decays on characteristic time scales of the order of 1 ps, while a residual population of ≈10% persists up to the maximum investigated pump-probe delay of 15 ps. The observation of a fast component is at variance with the results of other time-domain studies of $2H$-MoS_2 [28–31], which have all been conducted using bulk-sensitive trAOS. A similarly fast component was, however, reported in studies of few-layer and monolayer MoS_2 [18,21,22,25–27,29] indicating that, in contrast to the bulk material, hot carrier relaxation at $2H$-MoS_2 surfaces is largely governed by defect and surface state capture of charge carriers.

II. EXPERIMENT

For our study, commercially available and natural molybdenite crystals ($2H$-MoS_2, Manchester Nanomaterials Ltd.) were cleaved under ultrahigh vacuum conditions (5×10^{-10} mbar). Data from two different sample cleaves were analyzed and are presented in this work. TrARPES measurements were performed at a pressure of 3×10^{-10} mbar in a pump-probe configuration using frequency-doubled (3.14 eV) pump pulses [31 fs pulse width (FWHM)] delivered by a 8 kHz Ti:sapphire multipass amplifier and 11 fs extreme-ultraviolet (22.1 eV) probe pulses from a 395-nm-driven high-harmonic-generation (HHG) source [37,38]. The area illuminated by pump and probe beam at the sample position was 4.5×10^4 μm^2 and 1.7×10^4 μm^2 (FWHM), respectively. The photoemission system is equipped with a hemispherical analyzer allowing a simultaneous detection of energy and momentum. The effective time and energy resolutions of the experiment are 33 fs and 240 meV, respectively. All measurements were performed at room temperature using *s*-polarized pulses and an absorbed (pump) fluence of 0.75 m J cm^{-2} corresponding to a photoexcited carrier density of $\approx10^{13}$ cm^{-2} per MoS_2 sandwich as estimated for an absorption coefficient of 10^5 cm^{-1} [39]. Prior to the pump-probe measurements, the sample was fine-positioned with respect to the pump pulse in order to minimize electron background due to multiphoton photoemission processes, which can be enhanced substantially in the presence of surface defects. This procedure is necessary to avoid pump pulse-induced space-charge effects which can seriously affect the energy and momentum distribution of the electrons photoemitted by the probe pulse [40]. Details of the experimental setup are described in Ref. [38].

III. RESULTS AND DISCUSSION

We monitor the excitation and relaxation pathways of electrons in $2H$-MoS_2 after photoexcitation by analyzing the transient photoelectron intensity of the conduction-band states at different positions in energy-momentum space. Reliable results on corresponding hole pathways in the valence band could not be achieved due to masking of the transient signal by the dominating photoemission background from the intrinsic valence-band population. We would like to note, however, that independent of momentum, an instantaneous and transient change in the valence-band energy was observed, indicative of a rigid band shift of (110 ± 40) meV towards lower binding energies. We associate this shift with a band renormalization in response to the photoexcitation, as has been reported in optical spectroscopy experiments on mono- and bilayer WS_2 [41]. In the following, all energies are referred to the energy of the conduction-band minimum (CBM) E_{CBM} at $0.53\bar{\Gamma}\bar{K}$, where $E - E_{CBM} = 0$ eV. E_{CBM} was determined with an accuracy of ±150 meV by comparing the recorded photoemission band maps to the results of band structure calculations [42]. Since the band gap of $2H$-MoS_2 is 1.29 eV, absorption of 3.14 eV photons can, in principle, result in a nascent population of

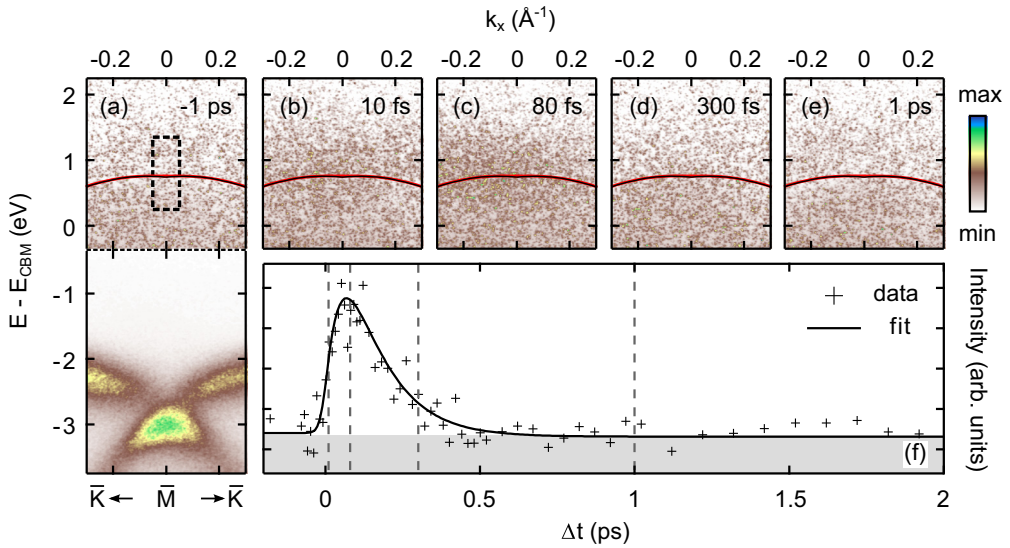

FIG. 2. TrARPES data of 2*H*-MoS_2 around $\overline{M}$. (a) ARPES intensity map of the valence (bottom) and conduction (top) band recorded with HHG light ($h\nu = 22.1$ eV) at 300 K in equilibrium, i.e., 1 ps before pump excitation. Separate color scales are used for the valence-band and conduction-band signal. (b)–(e) ARPES snapshots of the conduction-band region recorded at different time delays. For comparison, results of band structure calculations for the conduction band from Ref. [42] along the *M*-*K* (black line) and *L*-*H* (red line) direction are added. (f) Photoemission-intensity transient generated by integration of the photoemission signal over an energy and momentum region centered at $\overline{M}$, as indicated by the black dashed box in (a). The solid line is a fit to the experimental data by the model function described in the text. Dashed vertical lines mark the time delays of the snapshots shown in (b)–(e).

electronic states up to excess energies of 1.85 eV with respect to the CBM [see Fig. 4(a)].

Figures 2 and 3 show trARPES data recorded around $\overline{M}$ and 0.53 $\overline{\Gamma}\overline{K}$, respectively, illustrating the difference in the dynamics of the population of high- and low-energy states in the conduction band. The spectra in Fig. 2(a) depict photoemission data of the valence-band (bottom) and conduction-band (top) region around $\overline{M}$ prior to the absorption of the pump pulse, representing the undisturbed system. Changes in the photoemission intensity of the conduction band, reflecting the hot electron dynamics, are compared as snapshots at different pump-probe delays Δt in Figs. 2(b)–2(e). Figure 2(f) shows the transient of the photoemission intensity generated by integration over an energy and momentum region centered at $\overline{M}$ and an energy of $E - E_{\mathrm{CBM}} \approx 800$ meV [see dashed black box in Figs. 2(a) and 4(a)]. In this region, the intensity considerably increases already within the 31 fs duration of the pump pulse and reaches its maximum at $\Delta t \approx 80$ fs. At $\Delta t = 500$ fs, the excited-state population in the probed energy-momentum window has decayed almost completely.

The trARPES spectra along the $\overline{\Gamma}\overline{K}$ direction (center energy $E - E_{\mathrm{CBM}} \approx 450$ meV) are shown in Fig. 3 with the photoemission-intensity maps of the valence- and conduction-band region prior to the excitation in Fig. 3(a), characteristic snapshots of the conduction band in Figs. 3(b)–3(e), and the transient photoemission intensity around the CBM at 0.53 $\overline{\Gamma}\overline{K}$ in Fig. 3(f) [the integration region is marked by the dashed black box in Figs. 3(a) and 4(a)]. In contrast to the dynamics near $\overline{M}$, the increase in intensity at 0.53 $\overline{\Gamma}\overline{K}$ lasts for ≈180 fs, the intensity decay is slowed down to a picosecond time scale, and a residual intensity is still present at $\Delta t = 15$ ps. Furthermore, at 0.53 $\overline{\Gamma}\overline{K}$, we observe distinct changes in the energy-momentum distribution of the photoemission intensity: Whereas at $\Delta t = 80$ fs [Fig. 3(c)] the extended parabolic dispersion of the conduction band is visible, about 200 fs later [Fig. 3(d)], most of the intensity is concentrated near the CBM. These intensity changes reflect the successive relaxation of the hot electron distribution into the lowest-energy states of the conduction band, as further corroborated by the evolution of the momentum-integrated energy distribution curves shown in the inset of Fig. 3(f).

A. Data analysis

Quantitative information on the momentum-dependent excited-state dynamics is achieved by analyzing the experimental data as follows: Momentum-resolved conduction-band photoemission-intensity transients, as shown in Figs. 2(f) and 3(f), are generated for the different momentum cuts indicated in Fig. 1(b) with regions of integration spanning 0.05 to 0.1 Å^{-1} and 1.1 to 1.4 eV in the momentum and energy direction, respectively. Characteristic rise and decay times are determined by fitting the following model function to the transients:

$$I(t) = I_{01}, \quad \Delta t < t_0, \tag{1}$$

$$I(t) = I_{02} + A_1 \exp\left(-\frac{\Delta t - t_0}{\tau_{\mathrm{rise}}}\right) + A_2 \exp\left(-\frac{\Delta t - t_0}{\tau_{\mathrm{fall}}}\right), \quad \Delta t \geqslant t_0. \tag{2}$$

The two exponential functions describe the rise ($A_1 < 0$) and the fall ($A_2 > 0$) of the photoemission intensity

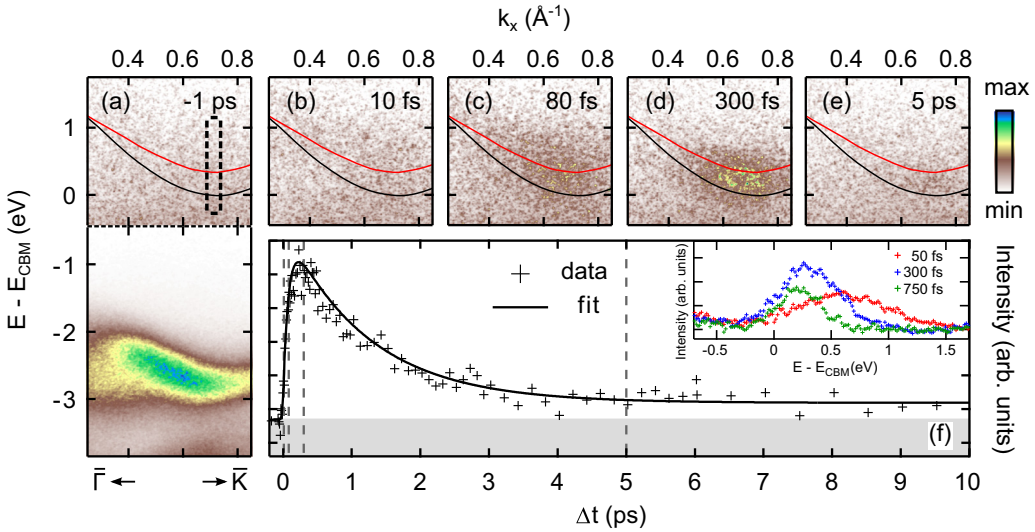

FIG. 3. TrARPES data of 2*H*-MoS_2 around 0.53 $\overline{\Gamma}\,\overline{K}$. (a) ARPES intensity map of the valence (bottom) and conduction (top) band recorded along the $\overline{\Gamma}\,\overline{K}$ direction with HHG light ($h\nu = 22.1$ eV) at 300 K in equilibrium, i.e., 1 ps before pump excitation. Separate color scales are used for the valence-band and conduction-band signal. (b)–(e) ARPES snapshots of the conduction band recorded at different time delays. For comparison, results of band structure calculations for the conduction band from Ref. [42] along the Γ-*K* (black line) and *A*-*H* (red line) direction are added. (f) Photoemission-intensity transient generated by integration of the photoemission signal over an energy and momentum region centered at 0.53 $\overline{\Gamma}\,\overline{K}$, as indicated by the black dashed box in (a). The solid line is a fit to the experimental data by the model function described in the text. Dashed vertical lines mark the time delays of the snapshots shown in (b)–(e). The inset compares energy distribution curves at different time delays obtained by integration of ARPES intensity maps along $\overline{\Gamma}\,\overline{K}$ ($0.35 \leqslant k_x \leqslant 0.85$ Å^{-1}).

corresponding to population and depopulation of excited states with the time constants τ_{rise} and τ_{fall}, respectively. I_{01} accounts for a constant overall background in the photoemission signal and I_{02} accounts for the residual electron population observed for some of the transients at the maximum investigated pump-probe delay of 15 ps. The parameter t_0 determines the onset time of population (and also depopulation) of the considered excited state. Notably, the fits do not yield any momentum dependence of t_0, indicating that the population of the conduction band starts globally within the temporal width of the excitation pulse. To ensure the continuity of the model function at t_0, the constraint $I_{01} = A_1 + A_2 + I_{02}$ is introduced. Finally, Eq. (1) is convolved with a squared secans hyperbolicus function (FWHM of 33 fs) representing the temporal resolution of the experiment. Fitting to the experimental data is performed with I_{01}, A_1, A_2, t_0, τ_{rise}, and τ_{fall} kept as free parameters. The model fully captures the observed dynamics, as evidenced by the results shown in Figs. 2(f) and 3(f).

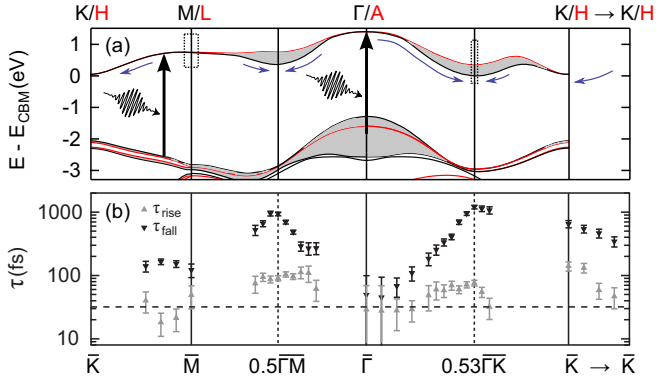

FIG. 4. (a) Calculated band structure of 2*H*-MoS_2 for the Γ*MK* (black) and *ALH* (red) planes, adopted from Ref. [42]. Black arrows indicate photoexcitation by absorption of 395 nm light. Blue arrows illustrate intraband relaxation of photoexcited electrons into the local conduction-band minima. The black dashed boxes indicate integration areas used to generate the photoemission-intensity transients shown in Figs. 2(f) and 3(f). (b) Characteristic photoemission-intensity rise times τ_{rise} and fall times τ_{fall} as a function of momentum, as determined from fits to momentum-dependent photoemission transients. The horizontal dashed line indicates the effective time resolution of the experiment (33 fs) as given by the FWHM of the pump-probe cross-correlation signal.

The fit results for τ_{rise} and τ_{fall} as a function of momentum are compiled in Fig. 4(b). For comparison, Fig. 4(a) also shows the calculated band structure of 2*H*-MoS_2 for the Γ*MK* and *ALH* plane [42]. Additional measurements have been performed in the vicinity of the conduction-band minima along $\overline{\Gamma}\,\overline{K}$ and $\overline{\Gamma}\,\overline{M}$ for absorbed pump fluences of 0.38 mJ cm^{-2} and 1.13 mJ cm^{-2} corresponding to photoexcited carrier densities of $\approx 5 \times 10^{12}$ cm^{-2} and $\approx 1.5 \times 10^{13}$ cm^{-2} per MoS_2 sandwich, respectively. Within this fluence range, no distinct dependence of τ_{rise} and τ_{fall} on the excitation density was observed. Also no indication for a dependence of τ_{rise} and τ_{fall} on the two different sample cleaves investigated in this study was observed.

B. Excitation and intraband relaxation

The results shown in Fig. 4 reveal that both τ_{rise} and τ_{fall} exhibit a momentum dependence that is highly correlated with the band structure of 2*H*-MoS_2. The lowest values of τ_{rise} are <30 fs, i.e., below the temporal resolution of the

experiment. They are observed at and close to $\overline{\Gamma}$ and $\overline{M}$, i.e., close to local maxima of the conduction-band dispersion. In the vicinity of these high-symmetry points and for an excitation photon energy of 3.14 eV, the band structure supports direct interband excitation from the valence band, as indicated by black arrows in Fig. 4(a). We may therefore associate the fast signal rise in the photoemission intensity with direct interband absorption that is responsible for the nascent population of the conduction band. The rise time τ_{rise} progressively increases as one approaches the local conduction-band minima at 0.53 $\overline{\Gamma}\overline{K}$, 0.5 $\overline{\Gamma}\overline{M}$, and $\overline{K}$ with maximum τ_{rise} values of ≈70, 90, and 140 fs, respectively. This indicates a delayed population by secondary processes. Notably, the characteristic rise times for the population of the local minima at 0.53 $\overline{\Gamma}\overline{K}$ and at $\overline{K}$ match strikingly well the decay times τ_{fall} observed for the nearby nascent population at $\overline{\Gamma}$ ($\tau_{\text{fall}} = 50$ fs) and $\overline{M}$ ($\tau_{\text{fall}} =$ 120 fs), respectively. The local minimum at 0.5 $\overline{\Gamma}\overline{M}$ adjoins both regions with nascent populations. Here, τ_{rise} approximately corresponds to the average of τ_{fall} at $\overline{\Gamma}$ and $\overline{M}$.

These observations suggest that the population of the conduction-band valleys occurs predominantly via energy relaxation of hot electrons out of the most proximate absorption region, as indicated by the blue arrows in Fig. 4(a). To ensure efficient energy relaxation of the nascent population towards the valley minima, scattering with small-momentum high-energy phonons needs to be involved. These relaxation processes may be driven by Fröhlich interaction with longitudinal optical phonons which, for monolayer MoS_2, have been shown to considerably contribute to hot electron cooling in the carrier density regime probed in the present study [43]. Carrier depopulation at $\overline{\Gamma}$ may in addition be promoted by impact ionization, as the excess energies with respect to the CBM are substantially larger than E_{gap} [42].

C. Depopulation of the conduction band

For the final decay of the excited-state population accumulated in the valley minima, the experimental data suggest the presence of at least two decay channels exhibiting considerably different efficiencies. The major part of the population decays on characteristic τ_{fall} time scales of ≈650 fs at $\overline{K}$, ≈900 fs at 0.5 $\overline{\Gamma}\overline{M}$, and ≈1.2 ps at 0.53 $\overline{\Gamma}\overline{K}$. For all three minima, a residual population is, however, visible even 15 ps after excitation, the maximum delay investigated in the present study [see Fig. 3(f)]. The appearance as a constant background in the recorded population transients implies that the time constant of this decay channel is significantly longer than 15 ps. The ratios between residual intensity and maximum intensity of the transients [see, e.g., Fig. 3(f)] are taken as a measure for the relative contribution of the slow decay component to the decay of the total population accumulated in the conduction-band minima. Analysis yields values of $9 \pm 4\%$, $13 \pm 3\%$, and $11 \pm 3\%$ for the minima at $\overline{K}$, 0.5 $\overline{\Gamma}\overline{M}$, and 0.53 $\overline{\Gamma}\overline{K}$, respectively. Correspondingly, the relative contributions of the fast component to the population decay are $91 \pm 4\%$, $87 \pm 3\%$, and $89 \pm 3\%$.

The depopulation of the conduction-band minima may arise either from intervalley scattering processes (restricted to $\overline{K}$ and 0.5 $\overline{\Gamma}\overline{M}$ due to energy conservation) or from scattering processes depopulating the conduction band as a whole. The latter processes particularly include carrier recombination and carrier capture by defect and surface states. Furthermore, carrier transport out of the probed volume may be effective, particularly in the case of a surface-sensitive experiment [36].

TrAOS studies of bulk MoS_2 [28–31] reported on sequential processes in the relaxation of photoexcited electrons, spanning time scales from a few-hundred fs to >4 ns. The assignment of these time scales to the different processes, however, appears to be difficult and not unambiguous. For instance, Kumar *et al.* [28] reported on intervalley scattering processes taking place within the first 350 fs after excitation and associated a 100 ps signature in the data with the depopulation of the conduction band. In contrast, Shi *et al.* [29] identified different types of intervalley scattering processes, with the fastest process being completed within a few picoseconds and the slowest one taking as long as 2.6 ns. According to that work, the final depopulation of the conduction band requires more than several nanoseconds. Similar time scales for intraband relaxation and conduction-band depopulation were also observed in Ref. [30]. Guo *et al.* [31] finally reported on the depopulation of the conduction band within 25 ps. In all of the above studies, carrier recombination has been considered as being exclusively responsible for the depopulation of the conduction band.

In the present trARPES study, we identify a distinct decay channel depopulating the global CBM at 0.53 $\overline{\Gamma}\overline{K}$ at a significantly shorter characteristic time scale of 1.2 ps. This additional pathway available for carrier relaxation from the conduction band has not been detected in trAOS so far.

Contrary to the reports on carrier dynamics in bulk MoS_2, several trAOS studies proved the existence of a fast depopulation channel for the conduction band in few-layer and monolayer MoS_2 [18,21,26,27,29]. The reported time scales range between 350 fs [27] and several picoseconds [21], in good agreement with the values for the fast depopulation component observed in the present study. The fast dynamics was attributed to carrier capture by defect states or surface states, a process that should be enhanced by the large surface-to-volume ratio of few-layer and monolayer samples in comparison to the bulk. We suspect that the extreme surface sensitivity of the trARPES technique makes it possible to probe similar processes taking place at the surfaces of MoS_2 bulk samples. Indeed, cleaved 2*H*-MoS_2 tends to exhibit a high density of surface defects, including steps generated in the cleaving process and localized defects such as vacancies and impurities. Past studies on structural defects of 2*H*-MoS_2 surfaces [44,45] revealed a rather inhomogeneous distribution with respect to species and density of defects. More specifically, high step density areas alternate with low step density areas on length scales of mm [44], whereas in the case of localized defect densities, variations between 0.1% and 10% have been reported with the density varying across very small areas of a size of 0.01 μm^2 [45]. We suspect that as a result of the adjustment of the sample position for a minimum of pump-induced multiphoton photoemission processes, a sample area exhibiting a rather low step density is probed in the experiment. We do not expect, however, a corresponding selectivity with respect to localized defects as their density substantially varies across length scales obviously much smaller than the size of the probe beam. Note

that the potential relevance of surface defect states for hot carrier relaxation at semiconductor surfaces has been pointed out before in time-resolved photoemission studies of GaAs and InP [46].

The observation of a second decay channel depopulating the conduction-band minima on time scales much longer than 15 ps is then only possible either in the case of saturation of the fast channel or in the presence of spatial inhomogeneities of the probed sample volume. As mentioned above, strong inhomogeneities in surface defect species and density have been reported for 2*H*-MoS_2 [45], potentially resulting in local variations of carrier capture rates [26,47–49] which would be probed in parallel in a spatially integrating trARPES experiment. This interpretation is consistent with different reports for monolayer MoS_2 [26,27,29]. The long-lived population component may alternatively arise from subsurface contributions to the photoemission signal dominated by bulk characteristic carrier-recombination processes, as predominantly probed in all-optical studies, i.e., indirect interband electron-hole recombination channels. Finally, diffusive transport of the electrons out of the probed sample volume may also contribute to the long-lived signal associated with the depopulation of the conduction band [50]. For an estimate of the related time scales, we have to take the crystalline anisotropy of 2*H*-MoS_2 into account and consider diffusion along the sandwich planes (governed by a diffusion constant $D_{\parallel} = 18\ \mathrm{cm^2\,s^{-1}}$ [28]) and perpendicular to the sandwich planes (diffusion constant $D_{\perp} < 10^{-2} \cdot D_{\parallel}$ [51,52]) separately. The spreading L of the electron distribution due to diffusion within a time interval Δt is given by $L = \sqrt{D \cdot \Delta t}$, with D being the corresponding diffusion constant. For the maximum time interval $\Delta t_{\mathrm{max}} = 15$ ps probed in the present study, this relation yields a value $L = 160$ nm for the in-plane spreading, i.e., a value which is negligible in comparison to the spot size of pump and probe beam, proving that in-plane diffusion does not affect our experimental data. For the spreading of the electron cloud perpendicular to the planes, a similar estimate yields a value $L < 16$ nm, which has to be compared to an excitation depth in 2*H*-MoS_2 of 20 nm for absorption of 400 nm light [51]. We conclude that diffusion perpendicular to the sandwich planes may start to affect our data at the maximum time delays Δt_{max} probed in our study.

In this context, we would like to refer to a time-resolved photoemission study of $MoSe_2$ and WSe_2 that reported on a fast depopulation of the conduction band on time scales of a few picoseconds [36]. These time scales were indeed associated with diffusion of electrons into the bulk. A quantitatively satisfactory description relied, however, on diffusion coefficients that exceeded the values reported for MoS_2 by a factor of 10 to 100.

IV. CONCLUSION

In conclusion, we presented a trARPES study of hot electron dynamics in the conduction band of photoexcited 2*H*-MoS_2. The unique capabilities of the used technique enabled us to directly monitor energy-momentum relaxation of excited carriers selectively within the surface region of the bulk material. We particularly point out the aspect of momentum resolution of the trARPES technique, which allows probing electron dynamics in the band structure in a direct way and particularly complements results achieved with all-optical techniques. Figure 5 schematically summarizes the identified excitation and relaxation pathways and the measured time scales. The analysis of the momentum-dependent photoemission transients allows us not only to locate optical interband transitions responsible for the generation of a nascent hot electron distribution, but also to track subsequent intraband relaxation pathways of the excited electrons in energy-momentum space. The conduction band is finally depopulated within ≈1 ps, with a residual population remaining for significantly longer times. Thus, in contrast to results of time-resolved studies of bulk 2*H*-MoS_2 using trAOS techniques [28–31], we observe a considerably accelerated depopulation of the conduction band. Instead, quantitative agreement with results for few-layer and monolayer MoS_2 is found [18,21,26,27,29]. Following the explanation given in the latter studies, we attribute the accelerated dynamics observed within our trARPES study to the presence of surface defects.

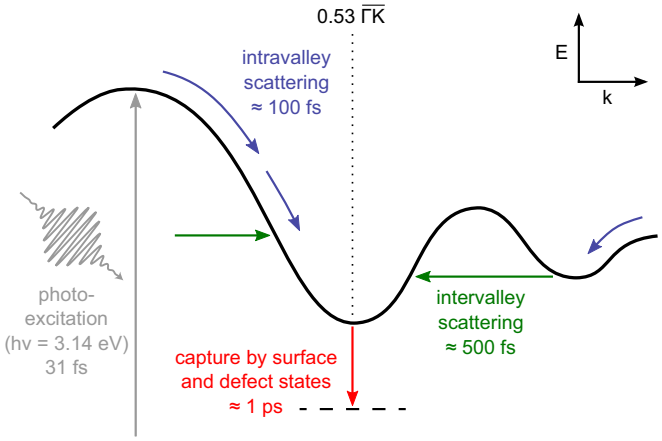

FIG. 5. Schematic illustration of relaxation pathways of hot electrons in the conduction band of 2*H*-MoS_2 after photoexcitation with 395 nm laser pulses, as identified within the present study.

Finally, we emphasize that the ARPES-based experiment presented here is another example in which the surface sensitivity of this technique is used to selectively probe aspects intimately related to the interesting physics of monolayers of transition-metal dichalcogenides, such as MoS_2 and WSe_2. More specifically, the impact of defects on carrier recombination highlight the exceeding relevance of defects for the peculiar optical properties of these two-dimensional materials [53].

ACKNOWLEDGMENTS

This work was supported by the Deutsche Forschungsgemeinschaft (DFG) through Project No. BA 2177/9-1. L.X.Y. is grateful to the Alexander von Humboldt Foundation for support.

[1] S. K. Mahatha, K. D. Patel, and K. S. R. Menon, J. Phys.: Condens. Matter **24**, 475504 (2012).

[2] Q. H. Wang, K. Kalantar-Zadeh, A. Kis, J. N. Coleman, and M. S. Strano, Nat. Nanotechnol. **7**, 699 (2012).

[3] S. Z. Butler, S. M. Hollen, L. Cao, Y. Cui, J. A. Gupta, H. R. Gutierrez, T. F. Heinz, S. S. Hong, J. Huang, A. F. Ismach, E. Johnston-Halperin, M. Kuno, V. V. Plashnitsa, R. D. Robinson, R. S. Ruoff, S. Salahuddin, J. Shan, L. Shi, M. G. Spencer, M. Terrones, W. Windl, J. E. Goldberger, H. R. Gutiérrez, T. F. Heinz, S. S. Hong, J. Huang, A. F. Ismach, E. Johnston-Halperin, M. Kuno, V. V. Plashnitsa, R. D. Robinson, R. S. Ruoff, S. Salahuddin, J. Shan, L. Shi, M. G. Spencer, M. Terrones, W. Windl, and J. E. Goldberger, ACS Nano **7**, 2898 (2013).

[4] R. S. Sundaram, M. Engel, A. Lombardo, R. Krupke, A. C. Ferrari, P. Avouris, and M. Steiner, Nano Lett. **13**, 1416 (2013).

[5] A. C. Ferrari, F. Bonaccorso, V. Falko, K. S. Novoselov, S. Roche, P. Bøggild, S. Borini, F. Koppens, V. Palermo, N. Pugno, J. A. Garrido, R. Sordan, A. Bianco, L. Ballerini, M. Prato, E. Lidorikis, J. Kivioja, C. Marinelli, T. Ryhänen, A. Morpurgo, J. N. Coleman, V. Nicolosi, L. Colombo, A. Fert, M. Garcia-Hernandez, A. Bachtold, G. F. Schneider, F. Guinea, C. Dekker, M. Barbone, C. Galiotis, A. Grigorenko, G. Konstantatos, A. Kis, M. Katsnelson, C. W. J. Beenakker, L. Vandersypen, A. Loiseau, V. Morandi, D. Neumaier, E. Treossi, V. Pellegrini, M. Polini, A. Tredicucci, G. M. Williams, B. H. Hong, J. H. Ahn, J. M. Kim, H. Zirath, B. J. van Wees, H. van der Zant, L. Occhipinti, A. Di Matteo, I. A. Kinloch, T. Seyller, E. Quesnel, X. Feng, K. Teo, N. Rupesinghe, P. Hakonen, S. R. T. Neil, Q. Tannock, T. Löfwander, and J. Kinaret, Nanoscale **7**, 4598 (2015).

[6] F. Bonaccorso, A. Lombardo, T. Hasan, Z. Sun, L. Colombo, and A. C. Ferrari, Mater. Today **15**, 564 (2012).

[7] K. F. Mak, C. Lee, J. Hone, J. Shan, and T. F. Heinz, Phys. Rev. Lett. **105**, 136805 (2010).

[8] E. Cappelluti, R. Roldán, J. A. Silva-Guillén, P. Ordejón, and F. Guinea, Phys. Rev. B **88**, 075409 (2013).

[9] T. Cao, G. Wang, W. Han, H. Ye, C. Zhu, J. Shi, Q. Niu, P. Tan, E. Wang, B. Liu, and J. Feng, Nat. Commun. **3**, 887 (2012).

[10] K. F. Mak, K. He, J. Shan, and T. F. Heinz, Nat. Nanotechnol. **7**, 494 (2012).

[11] X. Zhang, Q. Liu, J.-W. Luo, A. J. Freeman, and A. Zunger, Nat. Phys. **10**, 387 (2014).

[12] M. Gehlmann, I. Aguilera, G. Bihlmayer, E. Młyńczak, M. Eschbach, S. Döring, P. Gospodarič, S. Cramm, B. Kardynał, L. Plucinski, S. Blügel, and C. M. Schneider, Sci. Rep. **6**, 26197 (2016).

[13] J. M. Riley, F. Mazzola, M. Dendzik, M. Michiardi, T. Takayama, L. Bawden, C. Granerød, M. Leandersson, T. Balasubramanian, M. Hoesch, T. K. Kim, H. Takagi, W. Meevasana, P. Hofmann, M. S. Bahramy, J. W. Wells, and P. D. C. King, Nat. Phys. **10**, 835 (2014).

[14] R. Bertoni, C. W. Nicholson, L. Waldecker, H. Hübener, C. Monney, U. De Giovannini, M. Puppin, M. Hoesch, E. Springate, R. T. Chapman, C. Cacho, M. Wolf, A. Rubio, and R. Ernstorfer, arXiv:1606.03218.

[15] The natural form of 2*H*-MoS_2 is a $2H_b$ polytype.

[16] J. Shah, *Ultrafast Spectroscopy of Semiconductors and Semiconductor Nanostructures*, 2nd ed. Springer Series in Solid-State Sciences (Springer, New York, 1999).

[17] Z. Nie, R. Long, L. Sun, C.-C. Huang, J. Zhang, Q. Xiong, D. W. Hewak, Z. Shen, O. V. Prezhdo, and Z.-H. Loh, ACS Nano **8**, 10931 (2014).

[18] K. J. Czech, B. J. Thompson, S. Kain, Q. Ding, M. J. Shearer, R. J. Hamers, S. Jin, and J. C. Wright, ACS Nano **9**, 12146 (2015).

[19] Z. Nie, R. Long, J. S. Teguh, C.-C. Huang, D. W. Hewak, E. K. L. Yeow, Z. Shen, O. V. Prezhdo, and Z.-H. Loh, J. Phys. Chem. C **119**, 20698 (2015).

[20] R. Wang, B. A. Ruzicka, N. Kumar, M. Z. Bellus, H.-Y. Chiu, and H. Zhao, Phys. Rev. B **86**, 045406 (2012).

[21] Q. Wang, S. Ge, X. Li, J. Qiu, Y. Ji, and D. Sun, ACS Nano **7**, 11087 (2013).

[22] T. Korn, S. Heydrich, M. Hirmer, J. Schmutzler, and C. Schuller, Appl. Phys. Lett. **99**, 102109 (2011).

[23] D. Lagarde, L. Bouet, X. Marie, C. R. Zhu, B. L. Liu, T. Amand, P. H. Tan, and B. Urbaszek, Phys. Rev. Lett. **112**, 047401 (2014).

[24] A. Grubišić Čabo, J. A. Miwa, S. S. Grønborg, J. M. Riley, J. C. Johannsen, C. Cacho, O. Alexander, R. T. Chapman, E. Springate, M. Grioni, J. V. Lauritsen, P. D. C. King, P. Hofmann, and S. Ulstrup, Nano Lett. **15**, 5883 (2015).

[25] S. Dal Conte, F. Bottegoni, E. A. A. Pogna, D. De Fazio, S. Ambrogio, I. Bargigia, C. D'Andrea, A. Lombardo, M. Bruna, F. Ciccacci, A. C. Ferrari, G. Cerullo, and M. Finazzi, Phys. Rev. B **92**, 235425 (2015).

[26] H. Wang, C. Zhang, and F. Rana, Nano Lett. **15**, 339 (2014).

[27] C. J. Docherty, P. Parkinson, H. J. Joyce, M.-H. Chiu, C.-H. Chen, M.-Y. Lee, L.-J. Li, L. M. Herz, and M. B. Johnston, ACS Nano **8**, 11147 (2014).

[28] N. Kumar, J. He, D. He, Y. Wang, and H. Zhao, J. Appl. Phys. **113**, 133702 (2013).

[29] H. Shi, R. Yan, S. Bertolazzi, J. Brivio, B. Gao, A. Kis, D. Jena, H. G. Xing, and L. Huang, ACS Nano **7**, 1072 (2013).

[30] J. H. Strait, P. Nene, and F. Rana, Phys. Rev. B **90**, 245402 (2014).

[31] X. Guo, H. Chen, X. Wen, and J. Zheng, J. Chem. Phys. **142**, 212447 (2015).

[32] I. Gierz, J. C. Petersen, M. Mitrano, C. Cacho, I. C. E. Turcu, E. Springate, A. Stöhr, A. Köhler, U. Starke, and A. Cavalleri, Nat. Mater. **12**, 1119 (2013).

[33] J. C. Johannsen, S. Ulstrup, F. Cilento, A. Crepaldi, M. Zacchigna, C. Cacho, I. C. Edmond Turcu, E. Springate, F. Fromm, C. Raidel, T. Seyller, F. Parmigiani, M. Grioni, and P. Hofmann, Phys. Rev. Lett. **111**, 027403 (2013).

[34] A. Stange, C. Sohrt, L. X. Yang, G. Rohde, K. Janssen, P. Hein, L.-P. Oloff, K. Hanff, K. Rossnagel, and M. Bauer, Phys. Rev. B **92**, 184303 (2015).

[35] A. Tanaka, N. J. Watkins, and Y. Gao, Phys. Rev. B **67**, 113315 (2003).

[36] A. Rettenberger, P. Leiderer, M. Probst, and R. Haight, Phys. Rev. B **56**, 12092 (1997).

[37] C. Sohrt, A. Stange, M. Bauer, and K. Rossnagel, Farad. Discuss. **171**, 243 (2014).

[38] S. Eich, A. Stange, A. Carr, J. Urbancic, T. Popmintchev, M. Wiesenmayer, K. Jansen, A. Ruffing, S. Jakobs, T. Rohwer, S. Hellmann, C. Chen, P. Matyba, L. Kipp, K. Rossnagel, M. Bauer, M. Murnane, H. Kapteyn, S. Mathias, and M. Aeschlimann, J. Electron Spectrosc. Relat. Phenom. **195**, 231 (2014).

[39] B. L. Evans and P. A. Young, Proc. R. Soc. London A **298**, 74 (1967).

[40] L.-P. Oloff, K. Hanff, A. Stange, G. Rohde, F. Diekmann, M. Bauer, and K. Rossnagel, J. Appl. Phys. **119**, 225106 (2016).
[41] A. Chernikov, C. Ruppert, H. M. Hill, A. F. Rigosi, and T. F. Heinz, Nat. Photon. **9**, 466 (2015).
[42] T. Cheiwchanchamnangij and W. R. L. Lambrecht, Phys. Rev. B **85**, 205302 (2012).
[43] K. Kaasbjerg, K. S. Bhargavi, and S. S. Kubakaddi, Phys. Rev. B **90**, 165436 (2014).
[44] S. K. Mahatha and K. S. R. Menon, J. Phys.: Condens. Matter **24**, 305502 (2012).
[45] R. Addou, L. Colombo, and R. M. Wallace, ACS Appl. Mater. Interfaces **7**, 11921 (2015).
[46] R. Haight, Surf. Sci. Rep. **21**, 275 (1995).
[47] J. S. Blakemore, Phys. Rev. **110**, 1301 (1958).
[48] G. K. Wertheim, Phys. Rev. **109**, 1086 (1958).
[49] S. C. Choo, Phys. Rev. B **1**, 687 (1970).
[50] L. X. Yang, G. Rohde, T. Rohwer, A. Stange, K. Hanff, C. Sohrt, L. Rettig, R. Cortés, F. Chen, D. L. Feng, T. Wolf, B. Kamble, I. Eremin, T. Popmintchev, M. M. Murnane, H. C. Kapteyn, L. Kipp, J. Fink, M. Bauer, U. Bovensiepen, and K. Rossnagel, Phys. Rev. Lett. **112**, 207001 (2014).
[51] J. Wilson and A. Yoffe, Adv. Phys. **18**, 193 (1969).
[52] W. Kautek, H. Gerischer, and H. Tributsch, J. Electrochem. Soc. **127**, 2471 (1980).
[53] M. Amani, D.-H. Lien, D. Kiriya, J. Xiao, A. Azcatl, J. Noh, S. R. Madhvapathy, R. Addou, S. KC, M. Dubey, K. Cho, R. M. Wallace, S.-C. Lee, J.-H. He, J. W. Ager III, X. Zhang, E. Yablonovitch, and A. Javey, Science **350**, 1065 (2015).